

This document is confidential and is proprietary to the American Chemical Society and its authors. Do not copy or disclose without written permission. If you have received this item in error, notify the sender and delete all copies.

Modeling dispersal of UV filters in estuaries

Journal:	<i>Environmental Science & Technology</i>
Manuscript ID	es-2018-037255.R2
Manuscript Type:	Article
Date Submitted by the Author:	17-Dec-2018
Complete List of Authors:	Lindo-Atichati, David; Woods Hole Oceanographic Institution, Montero, Pedro; INTECMAR, Xunta de Galicia Rodil, Rosario; Univ Santiago de Compostela, Instituto de investigación y análisis alimentario Quintana, Jose Benito; University of Santiago de Compostela, Department of Analytical Chemistry, Nutrition and Food Sciences Miró, Manuel; University of the Balearic Islands, Chemistry

SCHOLARONE™
Manuscripts

Modeling dispersal of UV filters in estuaries

David Lindo-Atichati,^{*,†,‡,¶} Pedro Montero,[§] Rosario Rodil,^{||} José Benito Quintana,^{||} and Manuel Miró[⊥]

[†]*Department of Applied Ocean Physics and Engineering, Woods Hole Oceanographic Institution, Woods Hole, MA USA*

[‡]*Department of Earth and Planetary Sciences, American Museum of Natural History, New York, NY USA*

[¶]*Department of Engineering and Environmental Science, The City University of New York, Staten Island, NY USA*

[§]*INTECMAR, Xunta de Galicia, Vilagarcía de Arousa, Spain*

^{||}*Department of Analytical Chemistry, University of Santiago de Compostela, Santiago de Compostela, Spain*

[⊥]*FI-TRACE group, Department of Chemistry, University of the Balearic Islands, Carretera de Valldemossa km 7.5, E-07122 Palma de Mallorca, Spain*

E-mail: dlindo@whoi.edu

Abstract

Lagrangian ocean analysis, where virtual parcels of water are tracked through hydrodynamic fields, provides an increasingly popular framework to predict the dispersal of water parcels carrying particles and chemicals. We conduct the first direct test of Lagrangian predictions for emerging contaminants using: (1) the latitude, longitude, depth, sampling date, and concentrations of UV filters in raft cultured mussel (*Mytilus galloprovincialis*) of the estuary Ria de Arousa, Spain (42.5°N, 8.9°W); (2) a hydrodynamic numerical model at 300 m spatial resolution; and (3) a Lagrangian dispersion

9 scheme to trace polluted water parcels back to pollution sources. The expected dis-
10 persal distances (mean \pm SD) are 2 ± 1 km and the expected dispersal times (mean \pm
11 SD) are 6 ± 2 h. Remarkably, the probability of dispersal of UV filters from potential
12 sources to rafts decreases fivefold over 5 km. In addition to predicting dispersal path-
13 ways and times, this study also provides a framework for quantitative investigations
14 of concentrations of emerging contaminants and source apportionment using turbulent
15 diffusion. In the coastline, the ranges of predicted concentrations of the UV-filters
16 4-methylbenzylidene-camphor, octocrylene, and benzophenone-4 are $3.2 \cdot 10^{-4}$ -0.023
17 ng/mL, $2.3 \cdot 10^{-5}$ -0.009 ng/mL, and $5.6 \cdot 10^{-4}$ -0.013 ng/mL, respectively. At the outfalls
18 of urban wastewater treatment plants these respective ranges increase to $8.9 \cdot 10^{-4}$ -0.07
19 ng/mL, $6.2 \cdot 10^{-5}$ -0.027 ng/mL, and $1.6 \cdot 10^{-3}$ -0.040 ng/mL.

20 INTRODUCTION

21 Understanding patterns of dispersal of organic contaminants in aquatic environments is a
22 major goal of twenty-first century environmental science and technology¹⁻⁴. These patterns
23 determine the probability of contamination, and the pathways between pollution sources
24 and extremely valuable aquatic ecosystems^{5,6}. The pathways of contaminants, in turn, have
25 major implications for understanding environmental and health risks, and developing moni-
26 toring and mitigation strategies⁷⁻⁹.

27 The propagation of persistent organic pollutants (POPs) in natural environments has
28 emerged as a major issue for the last six decades. Persistent legacy organic contami-
29 nants (LOCs) include, for example, polycyclic aromatic hydrocarbons and polychlorinated
30 biphenyls. Due to their persistence, bioaccumulation, and environmental health risks¹⁰,
31 LOCs have been banned or severely restricted under international regulations¹¹. While
32 LOCs are still under close environmental scrutiny, the past two decades have also witnessed
33 the advent of POPs of concern. Persistent emerging organic contaminants (EOCs) encom-
34 pass a variety of bioaccumulative chemicals that are not covered by existing water-quality

35 regulations, and have the potential to enter the environment and cause adverse ecological
36 and (or) human health effects¹²⁻¹⁴. EOCs enter natural waters through urban and indus-
37 trial sewage, erosional runoff, leaching from agricultural areas and effluents of wastewater
38 treatment plants¹⁵, as they are not entirely removed by conventional wastewater treatment
39 technologies. After their release into the aquatic environment, EOCs can reach several envi-
40 ronmental compartments including soil, groundwater, air, and biota^{16,17}. Their persistence
41 in the aquatic environment has the potential to cause adverse ecological and human health
42 effects as bioaccumulated EOCs are potentially carcinogenic, mutagenic, toxic for reproduc-
43 tion, or act as endocrine disrupters^{12,18}. Nevertheless, it is not until recently that joint efforts
44 have been made by the research community to provide a comprehensive list of EOCs that em-
45 braces more than 700 pollutants, their metabolites and transformation products^{6,19,20}. The
46 EOCs on this list include UV filters associated with the growth of tourism activities^{16,21}.
47 Despite recent research efforts to integrate EOCs into hydrodynamic models²², the paucity
48 of real *in situ* data has limited the incorporation of EOCs data into physical models to study
49 their transport and fate⁸.

50 The raft cultured blue mussel (*Mytilus galloprovincialis*) model offers a tractable sys-
51 tem to investigate the mechanism by which EOCs are dispersed from potential sources to
52 aquaculture sites. Raft mussels represent an extreme case of aggregation in which individ-
53 uals live along suspended growth ropes^{23,24}. In any given population of raft cultured *M.*
54 *galloprovincialis*, the location of the raft is known, tissue of individuals can be collected,
55 concentrations of different analytes can be determined by liquid chromatography–mass spec-
56 trometry (LC-MS) and gas chromatography–mass spectrometry (GC-MS) approaches²⁵⁻²⁷,
57 and concentrations of analytes can be averaged (see the Supporting Information). Because
58 we found the concentrations of UV filters to be the highest across EOCs in mussels, we chose
59 UV filters as the representatives EOCs for this work. Data of contaminants found in the
60 aquatic environment can be incorporated into a particle dispersion model that, coupled with
61 a hydrodynamic numerical model, allows us to trace polluted water parcels from sources to

62 potential destination sites and vice versa²⁸. The outputs of these Lagrangian models are 3D
63 coordinates of the polluted water parcels through time, thus enabling the computation of
64 dispersal distances, dispersal times, and connectivity matrices. The validity and state of the
65 Lagrangian integrated modeling approach has been recently reviewed by van Sebille et al.
66 2017²⁹. For example, a better understanding of the relative effects of hydrodynamic, ther-
67 modynamic, and geochemical factors on the fate and transport of oil plumes in the subsea
68 can be achieved by incorporating experimental and *in situ* data into Lagrangian modeling
69 frameworks³⁰. Although water quality models have been already applied to persistent or-
70 ganic pollutants (e.g. O’Driscoll et al. 2013³¹), few models have addressed the fate and
71 transport of emerging contaminants due to the limited available data²². Here, we incorpo-
72 rate these data into a stochastic Lagrangian model that is coupled with a high-resolution
73 hydrodynamic model to generate the expected trajectories of water parcels that transport
74 EOCs between pollution sources and mussel rafts that have been exposed. These results
75 enable us to derive dispersal distances, directions, times, expected concentrations of EOCs
76 at the shoreline, and the possible contamination sources and mechanisms that control the
77 transport and fate of dissolved contaminants in estuaries.

78 This is the first time that a particle tracking model is combined with chemical analysis of
79 organic contaminants in biota to track the sources and apportionment of EOCs in estuarine
80 settings.

81 MATERIALS AND METHODS

82 Study Site

83 The Galician Rias are a group of coastal embayments located in the West of Galicia (NW
84 Spain). They are situated along the northern boundary of the NW Africa upwelling sys-
85 tem^{32,33}. This fact together with the regional orography, has led Galician Rias to be the
86 second largest producer of blue mussel in the world, with nearly 267,000 tn annually³⁴. The

87 culture consists of wooden raft moorings with a maximum of 500 hanging ropes of a max-
88 imum length of 12 m where mussels grow. There are about 3,340 mussel rafts scattered
89 across the Galician Rias, most of them (around 2,300) in Ria de Arousa. This funnel-shaped
90 estuary has an average channel width of 9 km and a total channel length from mouth to
91 the most distant headwater tributary of 33 km. The inner part of the ria is less than 20 m
92 deep while, in the outer part of the ria, Salvora island divides the oceanic entrance into a
93 narrow and shallow northern mouth of approximately 10 m deep and a wider and deeper
94 southern mouth, approximately 55 m deep³⁵. This study was conducted using 67 locations
95 of potential sources of EOCs, and samples from a population of the raft cultured mussel
96 collected during four different seasons at 2 locations of Ria de Arousa (Figure 1).

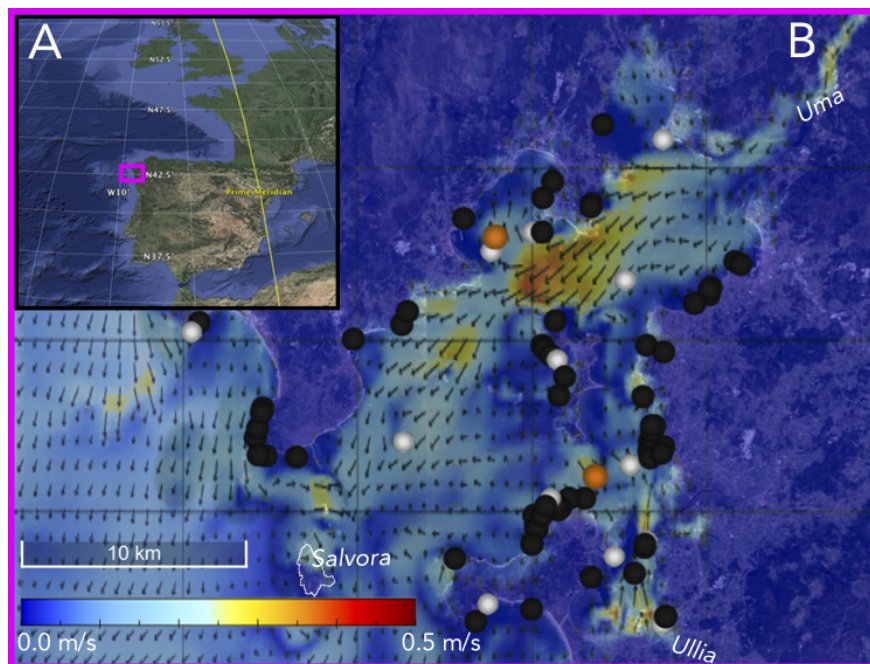


Figure 1: (a) Location of Ria de Arousa in the eastern North Atlantic. (b) Location of 2 mussel rafts (orange circles), marine outfalls of 11 wastewater treatment plants (white circles), and 56 industrial wastewater discharges (black circles) in Ria de Arousa.

97 The oceanographic structure of the ria is usually classified as a partially mixed. The tidal
98 forcing is mainly semidiurnal with M2 amplitude of about 1.1 m modulated over the spring-
99 neaps cycle by S2 and N2 amplitudes of about 0.3 m³⁶. The two main rivers that discharge
100 into this ria are the Ulla and the Umia, which have lower discharge rates in summer than in

101 any other season. In winter, stratification is determined by the river freshwater input while,
102 in contrast with the classical definition of estuaries, stratification in summer is caused by
103 solar heating³⁷.

104 The oceanographic circulation of the ria is driven by the succession of upwelling and
105 downwelling events driven by the dominant shelf winds interacting with topography. Offshore
106 northerly winds induce upwelling, increase stratification, and prevail from March to October.
107 Onshore southerly winds induce downwelling, reduce stratification, and dominate the rest
108 of the year. During upwelling winds, sub-surface central water intrudes as a lower layer
109 into the ria; during downwelling winds this colder lower layer disappears from the ria as
110 oceanic surface waters flow into the ria³⁸⁻⁴⁰. This seasonality mirrors the seasonally varying
111 changes in the strength and position of the atmospheric pressure cells that govern the North
112 Atlantic climatology, the Azores High and the Greenland Low, defining two wind-featured
113 oceanographic seasons. It is likely that local direct winds, including diurnal cycles play a
114 secondary role³⁵. Apart from their role in vertical mixing, tidal excursions are dominant
115 in the innermost ria^{41,42}, but they likely play a minor role in longitudinal exchange in the
116 middle ria where tidal excursions are less than 5 km due to the widening (narrowing) of the
117 middle (inner) region of the ria⁴¹.

118 **Mussel Sampling and Lagrangian Tracking**

119 *M. galloprovincialis* were collected from two mussel rafts located in the inner part of Ria de
120 Arousa; a northern mussel raft located 1,450 m offshore at 42.61°N, 8.91°W; and a southern
121 mussel raft located 1,550 m offshore at 42.51°N, 8.85°W. The average depth of the ropes
122 where mussels grow is 6 m. Samples at the northern location were collected on January
123 31, 2012; May 14, 2012; August 23, 2012; and November 7, 2012. Samples at the southern
124 location were collected on February 2, 2012; May 14, 2012; August 23, 2012; and November
125 8, 2012. These dates are used as the initial times for the backtracking Lagrangian simulation.
126 A map of likely trajectories of UV filters was generated at the former sampling locations and

127 dates, and trajectories were tracked backward in time for 10 days

128 **Hydrodynamic model component**

129 In order to obtain current velocity fields to force the Lagrangian model in Ria de Arousa, we
130 used the hourly outputs of a high resolution, operational model run by the Galician meteorological
131 service MeteoGalicia (www.meteogalicia.gal). The Oceanographic Operational System
132 implemented by MeteoGalicia consists of two nested levels of hydrodynamic models that
133 run daily⁴³. The largest grid is modeled by the Regional Ocean Modeling System (ROMS)⁴⁴,
134 which covers the Northern Iberian Peninsula (38–46°N, 4–14°W), with a horizontal spatial
135 resolution of 1/50° (ca. 2.2 km) and 41 vertical layers. Baroclinic lateral boundary conditions
136 are prescribed by the Iberia Biscay Irish ocean forecast model distributed by Copernicus
137 Marine Environment Monitoring Service⁴⁵, with a horizontal spatial resolution of 1/36° (ca.
138 3.1 km) and 50 vertical layers. Tidal data is provided by OSU TOPEX/Poseidon Global Inverse
139 Solution⁴⁶. The ROMS model provides lateral boundary conditions for several higher
140 resolution grids covering Rias of Artabro, Muros, Arousa, and Pontevedra/Vigo. At this
141 level, the water modeling system is MODElo HIDrodinâmico (MOHID, www.mohid.com)⁴⁷.
142 MOHID is an open-source free-surface, baroclinic regional circulation model developed by
143 MARETEC, a research group at University of Lisbon, Portugal. The model uses incompressibility,
144 hydrostatic, Boussinesq, and Reynolds approximations to solve the 3-dimensional
145 Navier-Stokes equations. Vertical velocities are computed through the continuity equation
146 integrated over the entire water column. The turbulent vertical mixing is solved by mean of
147 the General Ocean Turbulence Model (GOTM, <http://www.gotm.net>). The spatial discretisation
148 is implemented using a finite-volume method, solved in an Arakawa C-grid structure,
149 with horizontal resolution of 1/300° (ca. 300 m), 35 vertical layers, and time step of 30
150 s. Surface boundary conditions for winds and atmospheric fluxes are prescribed by the
151 Weather Research and Forecasting (WRF, [https://www.mmm.ucar.edu/weather-research-](https://www.mmm.ucar.edu/weather-research-and-forecasting-model)
152 [and-forecasting-model](https://www.mmm.ucar.edu/weather-research-and-forecasting-model)) model, which is run by MeteoGalicia at 12 km resolution for ROMS

153 and at 4 km resolution for MOHID twice a day. Daily averages of flow and temperature of
154 the main rivers -Miño, Verdugo, Lerez, Umia, Ulla, Tambre and Eume- were provided by
155 the Soil Water Assessment Tool (SWAT, <http://swatmodel.tamu.edu>) to feed both hydrody-
156 namic models. In the case of Ria de Arousa grid, in addition to Ulla and Umia rivers inputs,
157 minor tributaries are taken into account. An accurate bathymetry was constructed based on
158 data from the Spanish Navy Hydrographic Institute. MOHID has been extensively calibrated
159 and validated with MyOcean product Sea Ultra High Resolution Sea Surface Temperature
160 Analysis, Argo float data from IFREMER (French Research Institute for Exploration of
161 the Sea) and data sets from coastal monitoring programs in the western Iberian coast^{47,48}.

162 The MOHID archives used herein for the Lagrangian simulations consist of the three-
163 dimensional current velocity fields for January 31 to February 22, 2012; May 14 to May 24,
164 2012; August 23 to September 2, 2012; and November 7 to November 18, 2012.

165 Lagrangian model component

166 The methodology followed in this study to model dispersal of UV filters is similar to the La-
167 grangian methodology presented by Lindo-Atichati et al. 2016. Broadly, Lagrangian ocean
168 analysis is aimed at estimating the trajectory of virtual fluid particles by making use of Eu-
169 lerian fluid information, i.e., the velocity field. Alternatively, the Eulerian approach is based
170 on describing fluid motion in a reference frame that is fixed in space, enabling accurate com-
171 putation of concentrations but not enabling the tracking of fluid parcels. Both Lagrangian
172 and traditional Eulerian modeling approaches are robust methods, under a computational
173 point of view, to simulate the dispersion of pollutants^{22,31}. Lagrangian models generally
174 give more accurate results in terms of identification of ocean eddy and coherent features^{50,51}
175 while Eulerian models demand a significantly lesser computational time⁵⁰. Here, MOHID
176 provided estimates of 3-D currents to the open-source Lagrangian framework Parcels²⁸, which
177 is aimed at Lagrangian analyses and designed to be efficient for the new generation of ocean
178 circulation models in the petascale age²⁹. At its core, computing Lagrangian trajectories is

179 equivalent to solving the following equation:

$$X(t + \Delta t) = X(t) + \int_t^{t+\Delta t} v(x, \tau) d\tau + \Delta X_s(t) \quad (1)$$

180 where $X(t)$ is the three-dimensional position of a water parcel —carried by isopycnal and
181 vertical transports from the average depth of the mussel raft— and $v(x, \tau)$ represents the
182 three-dimensional Eulerian velocity field from MOHID at that position. $\Delta X_s(t)$ is a change
183 in position due to stochastic noise that is added to the horizontal motion of water parcels
184 to represent subgrid scale motions following the random walk model (i.e., a zeroth-order
185 Markov process)⁵². Due to that stochastic noise —a diffusivity term that accounts for the
186 subgrid scale eddies not resolved by the model— we obtain a map of likely trajectories in
187 a probabilistic (not deterministic) fashion. The trajectory Eq. (1) is time-stepped using a
188 fourth-order Runge-Kutta scheme.

189 Because ocean currents are highly variable both spatially and temporally and because
190 sub-mesoscale flows are chaotic in nature, two water parcels deployed simultaneously at
191 the same location often follow very different paths⁵³. Also, because of the inherent chaotic
192 nature of nonlinear advection and the unresolved subgrid-scale processes in MOHID, it is
193 only statistically that the modeled flows can be compared to the real world flows⁵⁴. To
194 account for this indeterminacy, we produced an envelope of likely trajectories by generating
195 hourly releases of 100 synthetic water parcels⁵⁵ at each location of the mussel raft and at the
196 average depth of the mussel rope during the 24 h of the *in situ* sampling dates, generating
197 2,400 trajectories per mussel raft, 4,800 trajectories per sampling day (2,400 trajectories
198 x 2 mussel rafts), and 19,200 trajectories for the four sampling dates (4,800 trajectories
199 x 4 sampling dates) (Figure 2). Synthetic water parcels containing UV filters were tracked
200 backward in time for 10 days using an integration time step of 10 min. Pathways of simulated
201 trajectories were terminated when reaching a shoreline, the bottom topography boundary,
202 or the 10 days limit, whichever occurred first.

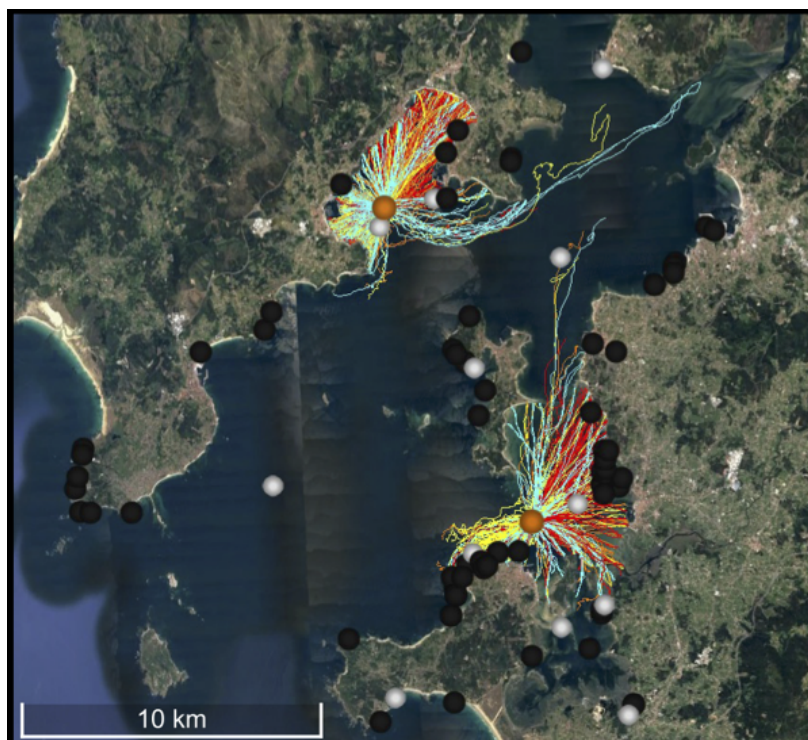


Figure 2: Simulated trajectories of water parcels released hourly at the mussel rafts locations (orange circles) on February 2, 2012 (cyan); May 14, 2012 (yellow); August 23, 2012 (red); and November 8, 2012 (orange). Trajectories are tracked backward in time for 10 days. To facilitate visualization, only 500 trajectories are represented. Orange, white and black circles depict the location of 2 mussel rafts, marine outfalls of 11 wastewater treatment plants, and 56 industrial wastewater discharges.

203 **Statistical analyses**

204 To generate an expected distribution of dispersal distances we estimated the shortest distance
205 between the coordinates of the mussel rafts and the coordinates where the contaminants are
206 predicted to be originated. Further, the 19,200 pairs of coordinates from the backtracking
207 study were used to estimate the actual distribution of dispersal directions and the distribution
208 of dispersal times.

209 We used a repeated measures permutational multivariate analysis of variance (RM-
210 PERMANOVA)⁵⁶ to test for differences in distributions of dispersal distance, direction,
211 and time between between sampling locations and among sampling seasons. All multivari-
212 ate statistical analyses were carried out in the R environment (www.r-project.org), using the

213 vegan package (<https://github.com/vegandevs/vegan>).

214 To explore the independent effect of sampling location on distance and direction of dis-
215 persal of UV filters we used bivariate polar graphs. Working in polar coordinates helps to
216 understand the directional dispersal dependence of different locations. For example, these
217 graphs show how the contaminants' direction of origin and distance varied in the northern
218 and southern location of Ria de Arousa. A Generalized Additive Model (GAM) is used to
219 derive smooth surfaces for all bivariate polar graphs using the 'openair' open source tools⁵⁷.

220 For brevity, we defined the useful combination of dispersal and eventually reaching the
221 coastline by polluted water parcels as 'beaching'. We tested the hypothesis that the proba-
222 bility of beaching will decline as a function of dispersal distance, direction, and time using
223 a logistic model (JMP v. 14.0.1). The probability of beaching between the sampled mussel
224 rafts and coastline locations (0 or 1) was used as the dependent variable, whereas distance
225 (continuous), and direction (continuous) between the sampled mussel rafts and the coastline
226 were assumed as independent variables. This approach enabled us to test for the effect of
227 one variable (e.g. distance) while controlling statistically for the effect of other variables (e.g.
228 direction), and explore the effect of interactions between variables. Independent variables
229 were removed from the model in a backward stepwise fashion if they did not have a signif-
230 icant effect. We confirmed that the model generated this way was the same as the model
231 generated using a forward stepwise approach.

232 **Model application**

233 Finally, we carried out an exercise that tested the suitability of this work for real life ap-
234 plications. Using (1) turbulent diffusion theory for estuaries and coastal waters, (2) the
235 spatial distribution and temporal evolution of polluted water parcels that were backtracked
236 in the Lagrangian simulations, and (3) the minimum and maximum concentrations of three
237 representative UV filters found in the mussels of the southern location of the estuary, we
238 computed estimates of the expected concentration of UV filters at the coastline and at the

239 outfalls of wastewater treatment plants.

240 Because Lagrangian models are not designed to calculate concentrations in a reference
 241 frame that is fixed in space, we calculated the concentration at the sources by using a solution
 242 of the equation of advective transport and molecular diffusion for turbulent flows:

243

$$\frac{\partial c}{\partial t} + u \frac{\partial c}{\partial x} + v \frac{\partial c}{\partial y} + w \frac{\partial c}{\partial z} = D \left(\frac{d^2 c}{dx^2} + \frac{d^2 c}{dy^2} + \frac{d^2 c}{dz^2} \right) \quad (2)$$

244

245 where c is the mass concentration, t is time, u is the velocity on the x-direction, v is
 246 the velocity on the y-direction, w is the velocity on the z-direction, and D is the molecular
 247 diffusion coefficient. The advective-diffusion equation is solved for estuaries and coastal
 248 waters assuming continuous line source of finite length⁵⁸ as sketched in Figure 3. This
 249 assumption is usually taken when wastewaters are discharged from outfalls with fairly long
 250 diffusers into essentially unbounded waters such as a wide estuary or coastal waters⁵⁹.

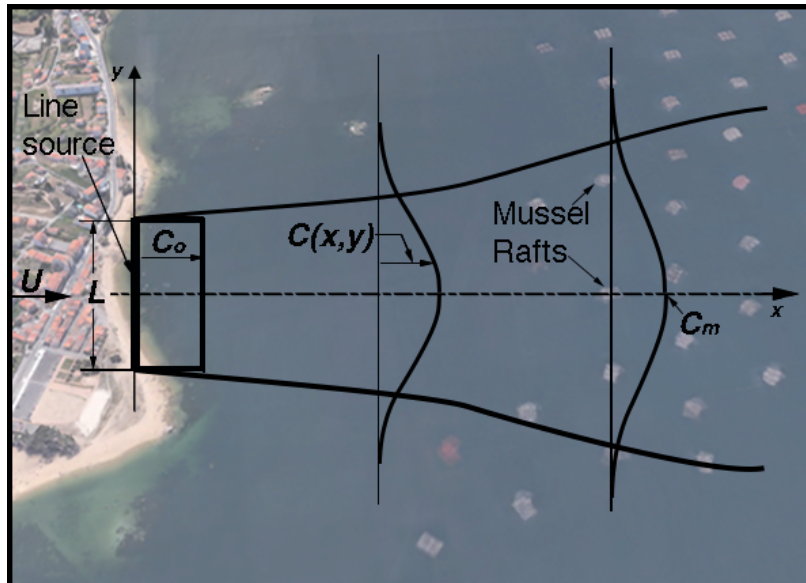


Figure 3: Diffusion of a contaminated fluid from a continuous line source of finite length L to mussel rafts of known concentration of UV filters C_m .

251

For this case, the advective-diffusion equation, Eq. 2, can be formulated as:

252

$$u \frac{\partial c}{\partial x} = \frac{\partial}{\partial x} \left(\epsilon_y \frac{\partial c}{\partial y} \right) \quad (3)$$

253

254 where ϵ_y is the diffusion coefficient on the y-direction. We assumed steady-state condi-
 255 tions, neglected diffusion in the x- and z-directions, and neglected bacterial decay. Solutions
 256 to Eq. 3 for various assumptions about the variation of ϵ_y were obtained by Brooks 1960⁶⁰,
 257 and derived for estuaries and coastal waters by Roberts and Webster 2002⁵⁸ obtaining the
 258 following equations:

259

$$C_o = C_m S_f \quad (4)$$

260

261

$$S_f = \left[\operatorname{erf} \left(\frac{3/2}{(1 + 8\alpha L^{-2/3} t)^3 - 1} \right)^{1/2} \right]^{-1} \quad (5)$$

262

263 where C_o [ng/mL seawater] is the expected initial concentration of contaminants assumed
 264 uniform along a line source, C_m [ng/mL seawater] is the maximum (centerline) concentration
 265 of contaminants in water parcels located at the sampled mussel raft, S_f is the far-field
 266 dilution, α is a constant depending on the energy dissipation rate that can be approximately
 267 bracketed with $0.01 < \alpha < 0.002 \text{ cm}^{2/3}/\text{s}$ and assumed as the upper value of $0.01 \text{ cm}^{2/3}/\text{s}$, L
 268 is the diffuser length [m] at the line source, t is the average dispersal time [h] of contaminants
 269 in water parcels from the mussel raft to the line source.

270

271

272

273

274

The diffuser length of the sources (L) and the average dispersal times from the mussel
 rafts to the sources (t) were obtained from the Lagrangian simulations. We considered two
 types of line sources; the coastline and the outfalls of urban wastewater treatment plants.
 The length of the coastal sources was the total distances of coastline that received polluted
 water parcels after 10 days of backtracking simulation. The diffuser length of the outfalls

275 was the number of outfalls that received at least one trajectory of polluted waters after 10
276 days of backtracking simulation multiplied by the minimum distance around the outfalls
277 that allows for detecting at least one trajectory. The diffuser lengths used in this work are
278 approximate estimates of the real diffuser lengths in the coastlines and outfalls of wastewater
279 treatment plants. A more precise computation of these L values is out of the scope of this
280 manuscript.

281 To represent the thermodynamic equilibrium between the organism and source compart-
282 ments we used the bioconcentration factor (BCF) specific for each UV filter in mussels.
283 Organisms can attain steady-state if both the exposure and the environmental/physiological
284 factors affecting the uptake and loss of pollutants remain constant for a sufficiently long
285 time. Thus, C_m can be calculated based on BCF as follows:

286

$$C_m = \frac{C_{mussel}}{BCF} \quad (6)$$

287

288 where C_{mussel} [ng/g dry weight] is the measured contaminant concentration in the mussel,
289 BCF [mL /g] is the measured bioconcentration factor in mussels⁶¹

290 We chose 4-methylbenzylidene-camphor (4-MBC: $C_{18}H_{22}O$), octocrylene (OC: $C_{24}H_{27}NO_2$),
291 and benzophenone-4 (BP-4: $C_{14}H_{12}O_6S$) as representative UV filters for this exercise of
292 model application. The reason for that choice is that bioaccumulation kinetics in *M. gallo-*
293 *provincialis*⁶² has been calculated, with mean BCF of 905 mL g⁻¹ for BP-4 and 2,210 mL
294 g⁻¹ for OC. The 4-MBC bioaccumulation did not fit a model due to the high variability of
295 the data and therefore we used a maximum BCF of 801 mL g⁻¹⁶².

296 RESULTS AND DISCUSSION

297 Modeled dispersal distances, directions, and times

298 Considering both sampling stations and all four sampling seasons, a total of 18,816 trajec-
 299 ries ended up in the coastline after 10 days of backtracking simulation. That is to say, at this
 300 spatial (300 m) and temporal (1 hr) resolution, 98 % of water parcels found near mussel rafts
 301 polluted with UV filters (located *ca.* 1,500 m offshore), likely originated from the coastline
 302 during the 10 days prior to collecting the mussels. The remaining 2 % of polluted water
 303 parcels either emanated from polluted sediments on the bottom of the estuary (1.2 %) or
 304 were continually flowing in the water column for more than 10 days prior to the sampling
 305 (0.8 %).

306 The distribution of trajectories revealed mean (mean \pm SD) dispersal distance, direction,
 307 and time of 2,090 \pm 1,090 m, 152 \pm 120°, and 6 \pm 2 h (Figure 4).

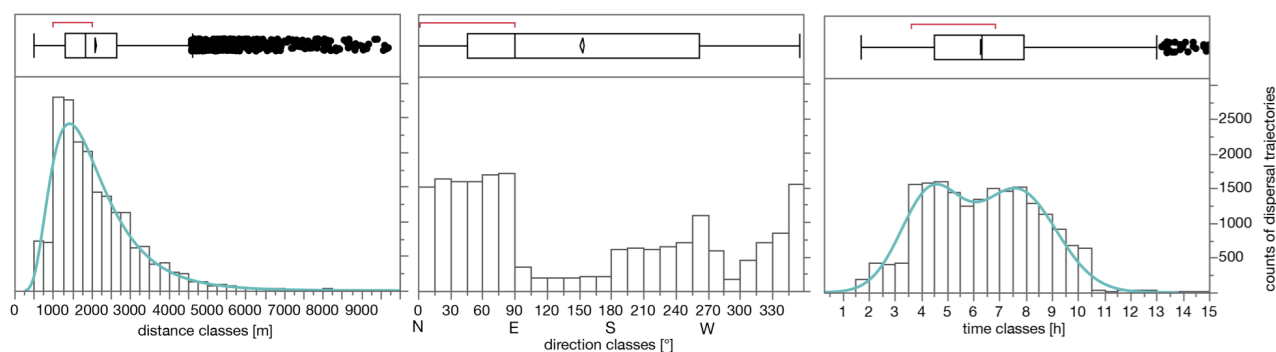


Figure 4: Distributions of dispersal distance, direction, and time of UV filters: determined by tracing water parcels back to sources in the coastline and offshore (white bars, $n = 19,200$). Counts of dispersal trajectories are the counts over 10 days in winter, spring, summer, and fall. To facilitate visualization, dispersal distances, directions, and times are assigned to 250 m, 15°, and 0.5 h bins, respectively. For each histogram, the rectangular box plot is delimited by the lower (Q1) and upper (Q3) quartiles, and the median is represented inside the box by a straight line. Whiskers are drawn to the extreme values that are inside the fences lying at $Q1 - [1.5 \times (Q3 - Q1)]$ and $Q3 + [1.5 \times (Q3 - Q1)]$. Potential outliers are marked with black circles. Red brackets defines the shortest half of the data (the densest region). Cyan lines represent the best continuous distribution (lowest AICc value) that fits to the data.

308 Although dispersal distances ranged from a few hundred meters up to 10,000 m, the distri-

309 bution was notably skewed, and fitted by a Johnson log-normal distribution (Komologorov-
 310 Smirnov-Lilliefors test: $p = 0.05$). Approximately 90 % of distances were less than 3,500 m,
 311 and the shortest interval that encompassed half of the data (the densest region) ranged from
 312 1000 to 2000 m. Noteworthy, less than 1 % of polluted water parcels reached the mussel
 313 rafts after having dispersed more than 5 km. Conversely, dispersal directions covered the
 314 full spectrum of angles; the shortest interval that encompassed half of the data (the densest
 315 region) ranged from 345 to 90° (north-northwest to east). Similar to dispersal distances,
 316 dispersal times ranged from 1 h up to 15 h; the distribution was primarily binomial; and
 317 best fitted by a mixture of two normal distributions (Normal-2 Mixture distribution: $\mu_1 =$
 318 4 h, $\mu_2 = 7$ h). The shortest interval that encompassed half of the data (the densest region)
 319 went from 3.5 to 6.5 h, which is within the tidal period for the region (12h).

320 We applied a logistic model to our independent variables and determined that probabil-
 321 ity of beaching was not random, the probability of beaching varied as a function of distance
 322 (Table 1 and Figure 5). Most strikingly, we found that the probability of contaminants origi-
 323 nating from the coastline declined significantly as the distance of the water parcel trajectory
 324 increased. UV filters were five times more likely to originate from distances between 500 m
 325 and 3,000 m than they were to originate at distances of 5,000 m. This suggests that the
 326 dispersal kernel of pollutants from mussels in estuaries is a unimodal leptokurtic distribution
 327 with a peak close to source.

Table 1: Probability of UV filters to reach the coastline in relation to multiple independent variables. Summary of the result of a stepwise logistic model that investigated the effects of distance, direction, and all interactions.

parameter	estimate	lower 95%	upper 95%	χ^2	$prob > \chi^2$
intercept	-6.7746	-7.6778	-5.9173	227.81	< 0.0001
distance	0.0027	0.0025	0.0028	1243.6	< 0.0001
direction	0.0005	-0.0012	0.0023	0.36	< 0.5461

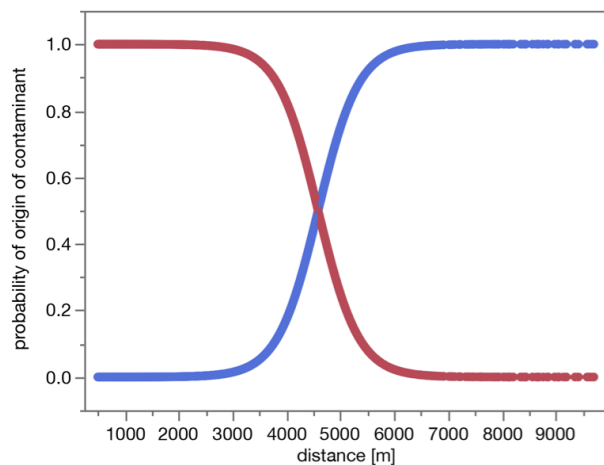


Figure 5: Probability of organic contaminant dispersal between the coastline (red curve) and raft mussels, and probability of organic contaminant dispersal between offshore locations (blue curve) and raft mussels. Curves are estimated from a logistic model (Table 1).

328 In contrast to the effect of distance, we found that the probability of beaching did not
329 vary consistently with the direction of origin of the seawater flow (Table 1). It should be
330 noted that it is possible that direction does not play a significant role in determining the
331 pattern of dispersal at this small spatial scale and due to the proximity of mussel rafts to
332 the coastline. We expect that current speeds will play a more significant role in determining
333 the pattern of dispersal at larger spatial scales and away from the inner ria⁴¹.

334 Effect of season and location

335 Considering the effect of season on the modeled trajectories of UV filters (Figure 2), we
336 observed that distributions of dispersal distance, direction, and time that we obtained from
337 the trajectories were not significantly different among the four seasons (RM-PERMANOVA:
338 global test: $p = 0.12$). Pairwise tests for every possible combination of seasons show no
339 significant differences between seasons for distributions of dispersal distance, direction, and
340 time at $p < 0.05$. However, the difference in the distribution of dispersal directions between
341 winter ($275 \pm 95^\circ$) and summer ($32 \pm 65^\circ$) was marginally significant at $p = 0.088$, and
342 was significant at $p = 0.1$. This marginal difference between the direction from which con-

343 taminants come in winter (approximately from the W) and summer (approximately from
344 the NNE) is in agreement with the two oceanographic season in the estuary and mirrors the
345 seasonality in wind fields and riverine outputs⁴⁰⁻⁴².

346 Considering the effect of raft location on the modeled trajectories of UV filters, we found
347 that distributions of dispersal distance, direction, and time were not significantly different be-
348 tween northern and southern sampling locations in the estuary (RM-PERMANOVA: global
349 test: $p = 0.1$). Pairwise tests show that distributions were not different between locations
350 at $p < 0.05$, with the exception of distributions of dispersal direction $p = 0.001$.

351 Bivariate polar plots, computed for distance-direction bins, illustrate the effect of location
352 on the envelope of distances and directions that contaminants traverse from the potential
353 sources to the mussel rafts (Figure 6). In the northern location of the estuary, mean per-
354 centage of trajectories of waters polluted with UV filters were very high (40% - 50%) in the
355 North to East quadrant, and pollutants came from sources located $1,900 \pm 1000$ m away
356 from the mussel raft (Figure 6a). Also in the northern location, mean percentage of trajec-
357 tories of waters polluted with UV filters were very high (40% - 50%) in the West direction,
358 and pollutants came from sources located $1,500 \pm 800$ m away from the mussel raft (Figure
359 6a). The most probable sources of UV-filters were the coastal locations that fell within the
360 former directions and distances, including 2 outfalls of wastewater treatment plants and 3
361 industrial wastewater discharges (Figure 6c). In the southern location of the estuary, mean
362 percentage of trajectories of waters polluted with UV filters were very high (40% - 50%) in
363 the Northeast direction, and pollutants came from sources located $1,800 \pm 950$ m away from
364 the mussel raft (Figure 6b). Also in the southern location, mean percentage of trajectories of
365 waters polluted with UV filters were very high (40% - 50%) in the West-Southwest direction,
366 and pollutants came from sources located $1,400 \pm 750$ m away from the mussel raft (Figure
367 6b). The most probable sources of UV-filters are the coastal locations that fall within the
368 former directions and distances, including 2 outfalls of wastewater treatment plants and 11
369 industrial wastewater discharges (Figure 6c). Noteworthy, 4 out of the 11 wastewater treat-

370 ment plants (36 %) and 14 out of the 56 industrial wastewater discharges (25 %) are within
 371 the potential foci of waters parcels polluted with UV-filters.

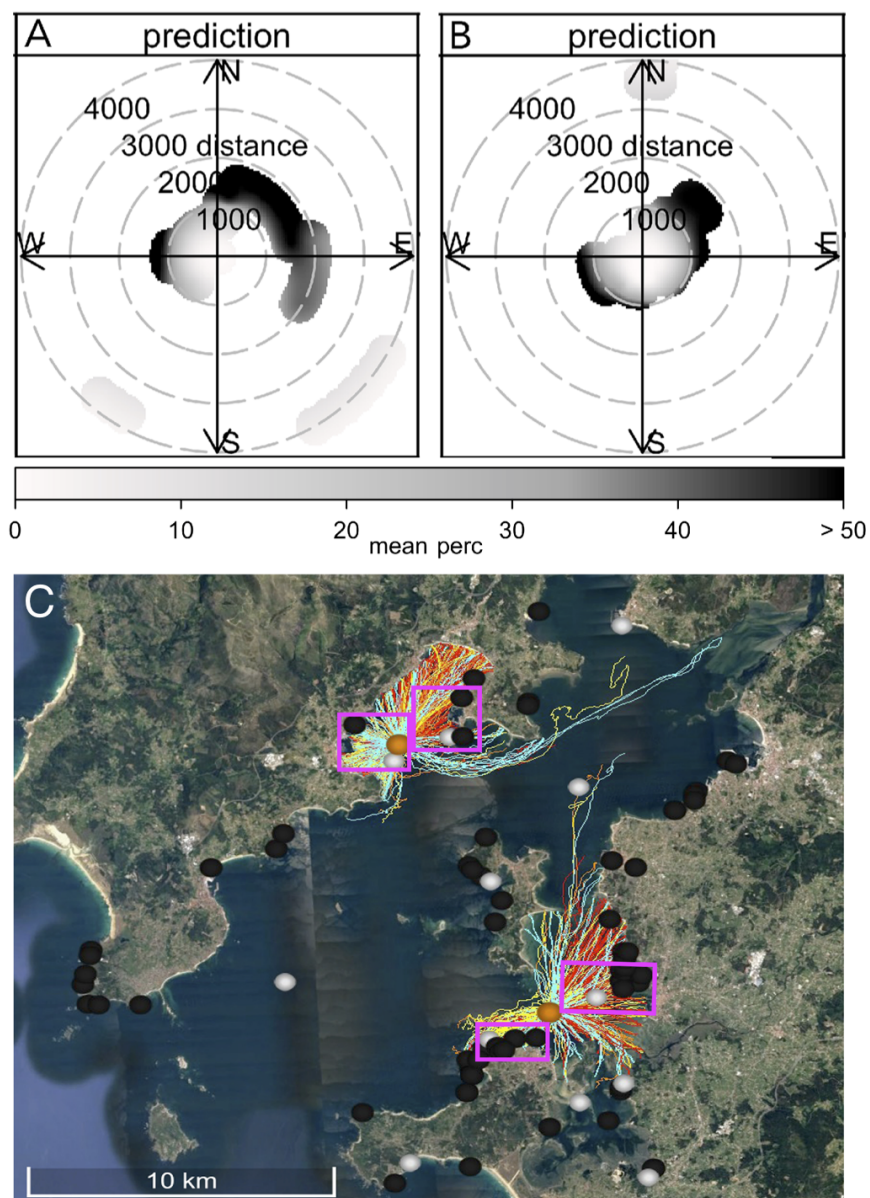


Figure 6: Bivariate polar plot of mean percentage of predicted trajectories in the northern (A) and southern (B) locations of the estuary. The key features of the northeast and southwest regions remain, suggesting that these features are “real” and not an artifact of potentially too few data. Simulated trajectories of water parcels polluted with UV filters (C) released on February (cyan), May (yellow), August (red), and November 2012 (orange). Orange, white and black circles depict the location of 2 mussel rafts, 11 wastewater treatment plants, and 56 industrial wastewater discharges. Purple rectangles depict the coastal that areas where most probable sources of UV-filters are located.

372 Modeled coastal concentrations and environmental implications

373 To test the suitability of this model for real life applications, we computed the expected
 374 concentration of the organic UV filters 4-MBC, OC and BP-4 in the coastline and in known
 375 locations of the outfalls of wastewater treatment plants⁶² that received polluted water parcels
 376 after 10 days of backtracking simulation. Then we compared the expected concentrations
 377 with *in situ* observations of concentrations of the three UV filters in wastewater treatment
 378 plants obtained from the literature²¹ (Table 2. We did not account for physicochemical pro-
 379 cesses because expected dispersal times t were very short compared with half-lives obtained
 380 from level III fugacity models⁶³.

Table 2: Minimum and maximum concentrations of organic UV filters in mussels and seawater of the sampled rafts (C_{mussel} s and C_m , this study), predicted minimum and maximum concentrations in the coastline and at the outfalls of urban wastewater treatment plants (C_o , this study), observed concentrations in seawater ($C_{seawater-ref}$, literature²¹), and observed concentrations in wastewater treatment plants. ($C_{wwtp-ref}$, literature²¹)

	4-MBC	OC	BP-4
mussel raft			
C_{mussel} [ng/g]	0.25-18	0.05-19	0.5-11.6
BCF [mL/g]	801	2,210	905
C_m [ng/mL]	$3.1 \cdot 10^{-4}$ -0.022	$2.2 \cdot 10^{-5}$ -0.008	$5.5 \cdot 10^{-4}$ -0.013
coastline			
L coastline [m]	12,000	12,000	12,000
t coastline [h]	5.8-5.9	5.4-5.9	5.8-5.9
S_f coastline [h]	1.013-1.014	1.010-1.014	1.013-1.014
C_o coastline [ng/mL]	$3.2 \cdot 10^{-4}$ -0.023	$2.3 \cdot 10^{-5}$ -0.009	$5.6 \cdot 10^{-4}$ -0.013
urban wwtp			
Number wwtp	7	7	7
Detection distance [m]	20	20	20
L [m]	70	70	70
t wwtp [h]	3.1-3.4	3.0-3.5	3.1-3.4
S_f wwtp [h]	2.84-3.09	2.76-3.18	2.84-3.09
C_o wwtp [ng/mL]	$8.9 \cdot 10^{-4}$ -0.07	$6.2 \cdot 10^{-5}$ -0.027	$1.6 \cdot 10^{-3}$ -0.040
seawater ²¹			
C_o [ng/mL]	n.d.-0.80	n.d.-2.78	<0.001
wwtp ²¹			
C_o [ng/mL]	n.d.-2.7	n.d.-0.2	n.d.-1.95

381 The range of concentrations and bioconcentration factor of 4-MBC in the southern mussel

382 raft were $C_m = 0.25\text{-}18$ ng/g dry weight and $\text{BCF} = 801$ mL g^{-1} . We carried out hourly
383 releases of 100 water parcels from the southern mussel raft located at 42.51°N , 8.85°W on
384 May 14, 2012 ($C_m = 0.25$ ng/g, minimum) and November 8, 2012 ($C_m = 18$ ng/g, maximum)
385 and traced them back for 10 days. The range of mean dispersal distance we obtained from
386 tracing back all 2,400 water parcels contaminated with 4-MBC to the coastline was 1,995-
387 2,020 m, while the mean dispersal distance we obtained from tracing back the water parcels
388 contaminated with 4-MBC to the outfalls of wastewater treatment plants was 1,600-1,710
389 m. The total distance of coastline that received polluted water parcels after 10 days of
390 backtracking simulation (diffuser length L) was 12,000 m. The total distance of outfalls
391 of urban wastewater treatment plants that received polluted water parcels after 10 days of
392 backtracking simulation (diffuser length L) was 140 m, which was computed using a detection
393 threshold distance of 20 m for each of the 7 outfalls. Using Eq. (4), Eq. (5) and Eq. (6)
394 we derived that the concentration of 4-MBC in the coastline and at the outfalls of urban
395 wastewater treatment plants were $C_o = 3.2 \cdot 10^{-4}\text{-}0.023$ ng/mL seawater and $C_o = 8.9 \cdot 10^{-4}\text{-}$
396 0.07 ng/mL, respectively. The upper limits of the predicted concentrations of 4-MBC in the
397 coastline and at the outfalls of urban wastewater treatment plants were within the ranges
398 of the observed concentrations of 4-MBC in seawater and in wastewater treatment plants²¹
399 (Table 2).

400 The range of concentrations and bioconcentration factor of OC in the southern mussel raft
401 were $C_m = 0.05\text{-}19$ ng/g dry weight and $\text{BCF} = 2,210$ mL g^{-1} . We carried out hourly releases
402 of 100 water parcels from the southern mussel raft located at 42.51°N , 8.85°W on May 14,
403 2012 ($C_m = 0.05$ ng/g, minimum) and February 2, 2012 ($C_m = 19$ ng/g, maximum) and
404 traced them back for 10 days. The range of mean dispersal distance we obtained from tracing
405 back all 2,400 water parcels contaminated with OC to the coastline was 1,995-2,010 m, while
406 the mean dispersal distance we obtained from tracing back the water parcels contaminated
407 with OC to the outfalls of wastewater treatment plants was 1,600-1,610 m. As with 4-MBC
408 and using Eq. (4), Eq. (5) and Eq. (6) we derived that the concentration of OC in the

409 coastline and at the outfalls of urban wastewater treatment plants were $C_o = 2.3 \cdot 10^{-5}$ -
410 0.009 ng/mL seawater and $C_o = 6.2 \cdot 10^{-5}$ - 0.027 ng/mL, respectively. The upper limits of
411 the predicted concentrations of OC in the coastline and at the outfalls of urban wastewater
412 treatment plants also were within the ranges of the observed concentrations of OC in seawater
413 and in wastewater treatment plants²¹ (Table 2).

414 The range of concentrations and bioconcentration factor of BP-4 in the southern mussel
415 raft were $C_m = 0.5$ - 11.6 ng/g dry weight and $BCF = 905$ mL g⁻¹. We carried out hourly
416 releases of 100 water parcels from the southern mussel raft located at 42.51°N, 8.85°W on
417 May 14, 2012 ($C_m = 0.5$ ng/g, minimum) and November 8, 2012 ($C_m = 11.6$ ng/g, maximum)
418 and traced them back for 10 days. The range of mean dispersal distance we obtained from
419 tracing back all 2,400 water parcels contaminated with BP-4 to the coastline was 1,995-
420 2,020 m, while the mean dispersal distance we obtained from tracing back the water parcels
421 contaminated with BP-4 to the outfalls of wastewater treatment plants was 1,600-1,710 m.
422 Using Eq. (4), Eq. (5) and Eq. (6) as in the above two target UV-filters we derived that the
423 concentration of BP-4 in the coastline and at the outfalls of urban wastewater treatment
424 plants were $C_o = 5.6 \cdot 10^{-4}$ - 0.013 seawater and $C_o = 1.6 \cdot 10^{-3}$ - 0.040 ng/mL, respectively.
425 The upper limits of the predicted concentrations of BP-4 in the coastline and at the outfalls
426 of urban wastewater treatment plants were one order of magnitude above and within the
427 ranges of the observed concentrations of BP-4 in seawater and in wastewater treatment
428 plants, respectively²¹ (Table 2).

429 A question should be raised regarding the toxicological relevance of the former observed
430 and predicted concentrations of three representative UV filters. How toxic are they for
431 mussels and for their coastal environment? Toxicity of organic and inorganic UV filters has
432 been demonstrated in aquatic organisms, and the occurrence of organic UV filters in molluscs
433 has been firmly established in ecotoxicological studies (e.g.,⁶⁴). Due to their lipophilicity,
434 these compounds tend to accumulate in muscle and adipose tissues of marine organisms⁶⁵.
435 For example, elevated concentrations of OC were found in mussels along the French coast (up

436 to 7112 ng/g d.w.), suggesting that bioaccumulation of organic UV-filters in the food webs
437 may be happening. Accumulated UV filters could be toxic for wild mussels and other species
438 in coastal environments^{64,66,67}. Paredes et al. 2014⁶⁸ evaluated the toxicity of 4-MBC, OC,
439 and BP-4 in *M. galloprovincialis*, *Paracentrotus lividus* (sea urchins) and *Siriella armata*
440 (crustacea). They found that 4-MBC and OC were the most toxic UV-filters whereas BP-4
441 presented the lowest toxicity; EC50 for 4-MBC ranged from a minimum of 192.63 ng/mL in
442 *S. armata* to a maximum of 853.74 ng/mL in *P. lividus* ; EC50 for OC ranged from 199.43
443 ng/mL in *S. armata* to 3118.18 ng/mL in *M. galloprovincialis*; EC50 for BP-4 was higher
444 than 10,000 ng/ mL in the three species.

445 Far-reaching environmental implications arise from the predicted levels of coastal con-
446 centrations of UV filters. Despite their persistence in the environment, UV filters are new
447 from an evolutionary point of view. Biota and microorganisms have not yet adapted their
448 metabolic pathways to efficiently degrade and remove them from the environment⁶⁹. There-
449 fore, organic UV filters also tend to accumulate in the environment, posing risk to the
450 ecosystem and the health of biota. Notably, these substances have a natural tendency to
451 accumulate in non-polar lipid tissues, consequently becoming persistent environmental con-
452 taminants that, biotransported through the food chain, can affect organisms on the higher
453 trophic levels, including humans⁷⁰.

454 In conclusion, recent advances in the field have led to the incorporation of emerging con-
455 taminants into simulation of pollutants' dispersal^{1,22}. Using a model that has been validated
456 from available observations helps to evaluate transport predictions and to parameterize the
457 horizontal eddy diffusivity of the Lagrangian framework⁴⁹. Our refined Lagrangian modeling
458 approach facilitates testing chemical and physical hypotheses for the factors concomitantly
459 influencing the pollutants dispersal, which will advance our understanding on pollution by
460 EOCs in the estuarine environment^{8,10,14,19}. To the best of our knowledge, this is the second
461 model that has been implemented to understand the fate and transport of emerging con-
462 taminants in estuaries. A hydrodynamic and emerging contaminant model was implemented

463 in Yangtze Estuary Reservoir and described the dynamic distributions of bisphenol-A in
464 the reservoir²². The outcome of our study is that a Lagrangian framework is able to pre-
465 dict meaningful dispersal distances, dispersal times, dispersal angles, seasonal variability in
466 transport, and concentrations of EOCs in estuarine environments. Furthermore, our results
467 demonstrate that, in estuarine systems, physical ocean processes influence the probability
468 that a particular dispersal trajectory will be taken. Specifically, the distance to the near-
469 est source of contamination, the oceanographic season in the estuary, the seasonality in
470 wind fields, and the riverine outflows are the main drivers of the transport of emerging
471 contaminants in estuaries. Incorporating more sampling data and additional estuaries into
472 the model⁶² will increase its explanatory power. Importantly, by developing a framework
473 for testing chemical and physical hypotheses in unison, this study lays the foundation for
474 a deeper understanding of dispersal of organic contaminants in the estuarine environment.
475 Given the occurrence of UV filters we found in mussels; the coastal and wastewater treat-
476 ment plant concentrations we modeled for 4-MBC, OC and BP-4; the known toxicity of the
477 former UV filters in the marine environment; and their potential effects on human health,
478 we recommend further ecotoxicological experiments, longterm exposure studies, and risk as-
479 sessment of organic UV filters in estuaries: from the affected biological sinks to the modeled
480 physical sources.

481 **Acknowledgement**

482 This research is supported by the Spanish State Research Agency projects CTM2014-56628-
483 C3-2-R, CTM2014-56628-C3-3-R, CTM2017-84763-C3-2-R, CTM2017-84763-C3-3-R, and CTM2017-
484 90890-REDT (MINECO/ AEI/FEDER, EU). The authors thank the Galician meteorological
485 service MeteoGalicia for providing the hydrodynamic model fields. This work used the Ex-
486 treme Science and Engineering Discovery Environment (XSEDE), which is supported by the
487 National Science Foundation grant number NSF-OCE170005. We thank Pablo Pita, Depart-

488 ment of Applied Economy of the University of Santiago de Compostela, for the photo of the
489 mussel raft included as part of the Table of Content graphic.

490 Supporting Information Available

491 Analytical methodology for determination of UV filters in mussels (PDF)

492 References

- 493 (1) Laender, F. D.; Hammer, J.; Hendriks, A. J.; Soetaert, K.; Janssen, C. Combining
494 monitoring data and modeling identifies PAHs as emerging contaminants in the Arctic.
495 *Environ. Sci. Technol.* **2011**, *45*, 9024–9029.
- 496 (2) Schnoor, J. L. Re-emergence of emerging contaminants. *Environ. Sci. Technol.* **2014**,
497 *48*, 11019–11020.
- 498 (3) Munoz, G.; Budzinski, H.; Labadie, P. Influence of Environmental Factors on the Fate of
499 Legacy and Emerging Per- and Polyfluoroalkyl Substances along the Salinity/Turbidity
500 Gradient of a Macrotidal Estuary. *Environ. Sci. Technol.* **2017**, *51*, 12347–12357.
- 501 (4) Lohmann, R.; Muir, D.; Zeng, E. Y.; Bao, L.-J.; Allan, I. J.; Arinaitwe, K.; Booij, K.;
502 Helm, P.; Kaserzon, S.; Mueller, J. F. Aquatic Global Passive Sampling (AQUA-GAPS)
503 revisited: first steps toward a network of networks for monitoring organic contaminants
504 in the aquatic environment. *Environ. Sci. Technol.* **2017**, *51*, 1060–1067.
- 505 (5) Barber, L. B.; Keefe, S. H.; Brown, G. K.; Furlong, E. T.; Gray, J. L.; Kolpin, D. W.;
506 Meyer, M. T.; Sandstrom, M. W.; Zaugg, S. D. Persistence and potential effects of
507 complex organic contaminant mixtures in wastewater-impacted streams. *Environ. Sci.*
508 *Technol.* **2013**, *47*, 2177–2188.

- 509 (6) Bradley, P. M.; Journey, C. A.; Romanok, K. M.; Barber, L. B.; Buxton, H. T.; Fore-
510 man, W. T.; Furlong, E. T.; Glassmeyer, S. T.; Hladik, M. L.; Iwanowicz, L. R. Ex-
511 panded target-chemical analysis reveals extensive mixed-organic-contaminant exposure
512 in US streams. *Environ. Sci. Technol.* **2017**, *51*, 4792–4802.
- 513 (7) Fairbairn, D. J.; Arnold, W. A.; Barber, B. L.; Kaufenberg, E. F.; Koskinen, W. C.;
514 Novak, P. J.; Rice, P. J.; Swackhamer, D. L. Contaminants of emerging concern: mass
515 balance and comparison of wastewater effluent and upstream sources in a mixed-use
516 watershed. *Environ. Sci. Technol.* **2015**, *50*, 36–45.
- 517 (8) Reemtsma, T.; Berger, U.; Arp, H. P. H.; Gallard, H.; Knepper, T. P.; Neumann, M.;
518 Quintana, J. B.; Voogt, P. d. Mind the Gap: Persistent and Mobile Organic Compounds
519 Water Contaminants That Slip Through. *Environ. Sci. Technol.* **2016**, *50*, 10308–10315.
- 520 (9) Massei, R.; Busch, W.; Wolschke, H.; Schinkel, L.; Bitsch, M.; Schulze, T.; Krauss, M.;
521 Brack, W. Screening of pesticide and biocide patterns as risk drivers in sediments of major
522 European rivers mouths: ubiquitous or river basin-specific contamination? *Environ.*
523 *Sci. Technol.* **2018**, *52*, 2251–2260.
- 524 (10) Sun, M.; Arevalo, E.; Strynar, M.; Lindstrom, A.; Richardson, M.; Kearns, B.; Pick-
525 ett, A.; Smith, C.; Knappe, D. R. Legacy and emerging perfluoroalkyl substances are
526 important drinking water contaminants in the Cape Fear River Watershed of North
527 Carolina. *Environ. Sci. Technol. Lett.* **2016**, *3*, 415–419.
- 528 (11) Carlson, D. L.; Vault, D. S. D.; Swackhamer, D. L. On the rate of decline of persistent
529 organic contaminants in lake trout (*Salvelinus namaycush*) from the Great Lakes, 1970-
530 2003. *Environ. Sci. Technol.* **2010**, *44*, 2004–2010.
- 531 (12) Richardson, S. D.; Kimura, S. Y. Water analysis: emerging contaminants and current
532 issues. *Anal. Chem.* **2015**, *88*, 546–582.

- 533 (13) Galimany, E.; Wikfors, G. H.; Dixon, M. S.; Newell, C. R.; Meseck, S. L.; Henning, D.;
534 Li, Y.; Rose, J. M. Cultivation of the Ribbed Mussel (*Geukensia demissa*) for Nutrient
535 Bioextraction in an Urban Estuary. *Environ. Sci. Technol.* **2017**, *51*, 13311–13318.
- 536 (14) Richardson, S. D.; Temes, T. A. Water analysis: Emerging contaminants and current
537 issues. *Anal. Chem.* **2018**, *90*, 398–428.
- 538 (15) Chiaia-Hernandez, A. C.; Krauss, M.; Hollender, J. Screening of lake sediments for
539 emerging contaminants by liquid chromatography atmospheric pressure photoionization
540 and electrospray ionization coupled to high resolution mass spectrometry. *Environ. Sci.*
541 *Technol.* **2012**, *47*, 976–986.
- 542 (16) Zedda, M.; Zwiener, C. Is nontarget screening of emerging contaminants by LC-HRMS
543 successful? A plea for compound libraries and computer tools. *Anal. Bioanal. Chem.*
544 **2012**, *403*, 2493–2502.
- 545 (17) Ismail, N. S.; Müller, C. E.; Morgan, R. R.; Luthy, R. G. Uptake of contaminants
546 of emerging concern by the bivalves *Anodonta californiensis* and *Corbicula fluminea*.
547 *Environ. Sci. Technol.* **2014**, *48*, 9211–9219.
- 548 (18) Loos, R.; Locoro, G.; Comero, S.; Contini, S.; Schwesig, D.; Werres, F.; Balsaa, P.;
549 Gans, O.; Weiss, S. Pan-European survey on the occurrence of selected polar organic
550 persistent pollutants in ground water. *Water Res.* **2010**, *44*, 4115–4126.
- 551 (19) Tiedeken, E. J.; Tahar, A.; McHugh, B.; Rowan, N. J. Monitoring, sources, receptors,
552 and control measures for three European Union watch list substances of emerging con-
553 cern in receiving waters—a 20 year systematic review. *Sci. Total Environ.* **2017**, *574*,
554 1140–1163.
- 555 (20) Environmental Protection Agency (EPA), Emerging Contaminants and Fed-
556 eral Facility Contaminants of Concern, Technical Fact Sheets. **2018**,

- 557 <https://www.epa.gov/fedfac/emerging-contaminants-and-federal-facility->
558 contaminants-concern (accessed April 20, 2018).
- 559 (21) Sánchez-Quiles, D.; Tovar-Sánchez, A. Are sunscreens a new environmental risk asso-
560 ciated with coastal tourism? *Environ. int.* **2015**, *83*, 158–170.
- 561 (22) Xu, C.; Zhang, J.; Bi, X.; Xu, Z.; He, Y.; Gin, K. Y.-H. Developing an integrated
562 3D-hydrodynamic and emerging contaminant model for assessing water quality in a
563 Yangtze Estuary Reservoir. *Chemosphere* **2017**, *188*, 218–230.
- 564 (23) Camacho, A. P.; Labarta, U.; Beiras, R. Growth of mussels (*Mytilus edulis galloprovin-*
565 *cialis*) on cultivation rafts: influence of seed source, cultivation site and phytoplankton
566 availability. *Aquaculture* **1995**, *138*, 349–362.
- 567 (24) Pérez-Camacho, A.; Labarta, U.; Vinseiro, V.; Fernández-Reiriz, M. J. Mussel produc-
568 tion management: raft culture without thinning-out. *Aquaculture* **2013**, *406*, 172–179.
- 569 (25) Schymanski, E. L.; Singer, H. P.; Slobodnik, J.; Ipolyi, I. M.; Oswald, P.; Krauss, M.;
570 Schulze, T.; Haglund, P.; Letzel, T.; Grosse, S. Non-target screening with high-
571 resolution mass spectrometry: critical review using a collaborative trial on water anal-
572 ysis. *Anal. Bioanal. Chem.* **2015**, *407*, 6237–6255.
- 573 (26) Llorca, M.; Farré, M.; Eljarrat, E.; Díaz-Cruz, S.; Rodríguez-Mozaz, S.; Wunderlin, D.;
574 Barcelo, D. Review of emerging contaminants in aquatic biota from Latin America:
575 2002–2016. *Environ. Toxicol. Chem.* **2017**, *36*, 1716–1727.
- 576 (27) Montesdeoca-Esponda, S.; Checchini, L.; Del Bubba, M.; Sosa-Ferrera, Z.; Santana-
577 Rodriguez, J. J. Analytical approaches for the determination of personal care products
578 and evaluation of their occurrence in marine organisms. *Sci. Total Environ.* **2018**, *633*,
579 405–425.

- 580 (28) Lange, M.; van Sebille, E. Parcels v0. 9: prototyping a Lagrangian ocean analysis
581 framework for the petascale age. *Geosci. Model Dev.* **2017**, *10*, 4175–4186.
- 582 (29) van Sebille, E.; Griffies, S. M.; Abernathey, R.; Adams, T. P.; Berloff, P.; Biastoch, A.;
583 Blanke, B.; Chassignet, E. P.; Cheng, Y.; Cotter, C. Lagrangian ocean analysis: fun-
584 damentals and practices. *Ocean Model.* **2017**, *121*, 49–75.
- 585 (30) Lindo-Atichati, D.; Paris, C.; Le Hénaff, M.; Schedler, M.; Juárez, A. V.; Müller, R.
586 Simulating the effects of droplet size, high-pressure biodegradation, and variable flow
587 rate on the subsea evolution of deep plumes from the Macondo blowout. *Deep Sea Res.*
588 *Part 2 Top. Stud. Oceanogr.* **2016**, *129*, 301–310.
- 589 (31) O’Driscoll, K.; Mayer, B.; Ilyina, T.; Pohlmann, T. Modelling the cycling of persistent
590 organic pollutants (POPs) in the North Sea system: fluxes, loading, seasonality, trends.
591 *J. Mar. Syst.* **2013**, *111*, 69–82.
- 592 (32) Wooster, W.; Bakun, A.; McLain, D. Seasonal upwelling cycle along the Eastern Bound-
593 ary of the North Atlantic. *J. Mar. Res.* **1976**, *34*, 131–141.
- 594 (33) Álvarez Salgado, X.; Figueiras, F.; Pérez, F.; Groom, S.; Nogueira, E.; Borges, A.;
595 Chou, L.; Castro, C.; Moncoiffé, G.; Ríos, A.; Miller, A.; Frankignoulle, M.; Savidge, G.;
596 Wollast, R. The Portugal coastal counter current off NW Spain: new insights on its
597 biogeochemical variability. *Prog. Oceanogr.* **2003**, *56*, 281 – 321.
- 598 (34) Gosling, E. *Marine Bivalve Molluscs*; Wiley-Blackwell, 2015; Chapter 9, pp 325–382.
- 599 (35) Bermúdez, M.; Pietrzak, J. D.; Cea, L.; Puertas, J.; Stelling, G. S.; De Boer, G. J.
600 A numerical study of mixing and stratification dynamics in the ría de Arousa estuary
601 (NW Spain) during summer. Coastal Dynamics 2013: 7th International Conference on
602 Coastal Dynamics, Arcachon, France, 24-28 June 2013. 2013.

- 603 (36) Cerralbo, P.; Grifoll, M.; Espino, M.; López, J. Predictability of currents on a mesotidal
604 estuary (Ria de Vigo, NW Iberia). *Ocean Dyn.* **2013**, *63*, 131–141.
- 605 (37) Alvarez-Salgado, X.; Gago, J.; Miguez, B.; Gilcoto, M.; Pérez, F. Surface waters of the
606 NW Iberian margin: upwelling on the shelf versus outwelling of upwelled waters from
607 the Rias Baixas. *Estuar. Coast. Shelf Sci.* **2000**, *51*, 821–837.
- 608 (38) Rosón, G.; Pérez, F. F.; Alvarez-Salgado, X.; Figueiras, F. Variation of both thermo-
609 haline and chemical properties in an estuarine upwelling ecosystem: Ria de Arousa; I.
610 time evolution. *Estuar. Coast. Shelf Sci.* **1995**, *41*, 195–213.
- 611 (39) Gilcoto, M.; Álvarez-Salgado, X.; Pérez, F. Computing optimum estuarine residual
612 fluxes with a multiparameter inverse method (OERFIM): application to the Ria de
613 Vigo (NW Spain). *J. Geophys. Res. Oceans* **2001**, *106*, 31303–31318.
- 614 (40) Piedracoba, S.; Álvarez-Salgado, X.; Rosón, G.; Herrera, J. Short-timescale thermoha-
615 line variability and residual circulation in the central segment of the coastal upwelling
616 system of the Ría de Vigo (northwest Spain) during four contrasting periods. *J. Geo-
617 phys. Res. Oceans* **2005**, *110*, 1–15.
- 618 (41) Barton, E.; Largier, J.; Torres, R.; Sheridan, M.; Trasviña, A.; Souza, A.; Pazos, Y.;
619 Valle-Levinson, A. Coastal upwelling and downwelling forcing of circulation in a semi-
620 enclosed bay: Ria de Vigo. *Prog. Oceanogr.* **2015**, *134*, 173–189.
- 621 (42) Gilcoto, M.; Largier, J. L.; Barton, E. D.; Piedracoba, S.; Torres, R.; Graña, R.; Alonso-
622 Pérez, F.; Villacieros-Robineau, N.; Granda, F. Rapid response to coastal upwelling in
623 a semienclosed bay. *Geophys. Res. Lett.* **2017**, *44*, 2388–2397.
- 624 (43) Costa, P.; Gómez, B.; Venâncio, A.; Pérez, E.; Pérez-Muñuzuri, V. Using the Regional
625 Ocean Modelling System (ROMS) to improve the sea surface temperature predictions
626 of the MERCATOR Ocean System. *Sci. Mar.* **2012**, *76*, 165–175.

- 627 (44) Shchepetkin, A. F.; McWilliams, J. C. The regional oceanic modeling system (ROMS):
628 a split-explicit, free-surface, topography-following-coordinate oceanic model. *Ocean*
629 *Model.* **2005**, *9*, 347–404.
- 630 (45) Sotillo, M. G.; Cailleau, S.; Lorente, P.; Levier, B.; Aznar, R.; Reffray, G.; Amo-
631 Baladrón, A.; Chanut, J.; Benkiran, M.; Alvarez-Fanjul, E. The MyOcean IBI Ocean
632 Forecast and Reanalysis Systems: operational products and roadmap to the future
633 Copernicus Service. *J. Oper. Oceanogr.* **2015**, *8*, 63–79.
- 634 (46) Egbert, G. D.; Erofeeva, S. Y. Efficient Inverse Modeling of Barotropic Ocean Tides.
635 *J. Atmospheric Ocean. Technol.* **2002**, *19*, 183–204.
- 636 (47) Mateus, M.; Riflet, G.; Chambel, P.; Fernandes, L.; Fernandes, R.; Juliano, M.; Cam-
637 puzano, F.; Pablo, H. d.; Neves, R. An operational model for the West Iberian coast:
638 products and services. *Ocean Sci.* **2012**, *10*, 713–732.
- 639 (48) Pinto, L.; Mateus, M.; Silva, A. Modeling the transport pathways of harmful algal
640 blooms in the Iberian coast. *Harmful algae* **2016**, *53*, 8–16.
- 641 (49) Lindo-Atichati, D.; Curcic, M.; Paris, C. B.; Buston, P. M. Description of surface trans-
642 port in the region of the Belizean Barrier Reef based on observations and alternative
643 high-resolution models. *Ocean Model.* **2016**, *106*, 74–89.
- 644 (50) Carvalho, J. C.; Vilhena, M. T.; Moreira, D. M. Comparison between Eulerian and
645 Lagrangian semi-analytical models to simulate the pollutant dispersion in the PBL.
646 *Appl. Math. Model.* **2007**, *31*, 120–129.
- 647 (51) Beron-Vera, F. J.; Wang, Y.; Olascoaga, M. J.; Goni, G. J.; Haller, G. Objective
648 detection of oceanic eddies and the Agulhas leakage. *J. Phys. Oceanogr.* **2013**, *43*,
649 1426–1438.
- 650 (52) Griffa, A. *Stochastic modelling in physical oceanography*; Springer, 1996; pp 113–140.

- 651 (53) LaCasce, J. Statistics from Lagrangian observations. *Prog. Oceanogr.* **2008**, *77*, 1–29.
- 652 (54) Mariano, A. J.; Griffa, A.; Özgökmen, T. M.; Zambianchi, E. Lagrangian analysis and
653 predictability of coastal and ocean dynamics 2000. *J. Atmospheric Ocean. Technol.*
654 **2002**, *19*, 1114–1126.
- 655 (55) Lynch, D. R.; Greenberg, D. A.; Bilgili, A.; McGillicuddy Jr, D. J.; Manning, J. P.;
656 Aretxabaleta, A. L. *Particles in the coastal ocean: Theory and applications*; Cambridge
657 University Press, 2014.
- 658 (56) Anderson, M. J. A new method for non-parametric multivariate analysis of variance.
659 *Austral Ecol.* **2001**, *26*, 32–46.
- 660 (57) Carslaw, D. C.; Ropkins, K. Openair—an R package for air quality data analysis.
661 *Environ. Model. Softw.* **2012**, *27*, 52–61.
- 662 (58) Roberts, P. J.; Webster, D. R. *Turbulent diffusion*; ASCE Press, Reston, Virginia, 2002.
- 663 (59) Roberts, P. J. *Environmental Hydraulics*; Springer, 1996; pp 63–110.
- 664 (60) Brooks, N. H. Diffusion of sewage effluent in an ocean current. *Waste disposal in the*
665 *marine environment* **1960**, 246–267.
- 666 (61) Landrum, P. F.; Lydy, M. J.; Lee, H. Toxicokinetics in aquatic systems: model com-
667 parisons and use in hazard assessment. *Environ. Toxicol. Chem.* **1992**, *11*, 1709–1725.
- 668 (62) Vidal-Liñán, L.; Villaverde-de Saa, E.; Rodil, R.; Quintana, J. B.; Beiras, R. Bioac-
669 cumulation of UV filters in *Mytilus galloprovincialis* mussel. *Chemosphere* **2018**, *190*,
670 267–271.
- 671 (63) Pence, H. E.; Williams, A. ChemSpider: an online chemical information resource. *J.*
672 *Chem. Educ.* **2010**, *87*, 1123–1124.

- 673 (64) Bachelot, M.; Li, Z.; Munaron, D.; Le Gall, P.; Casellas, C.; Fenet, H.; Gomez, E.
674 Organic UV filter concentrations in marine mussels from French coastal regions. *Sci.*
675 *Total Environ.* **2012**, *420*, 273–279.
- 676 (65) Gago-Ferrero, P.; Diaz-Cruz, M. S.; Barceló, D. An overview of UV-absorbing com-
677 pounds (organic UV filters) in aquatic biota. *Anal. Bioanal. Chem.* **2012**, *404*, 2597–
678 2610.
- 679 (66) Nakata, H.; Murata, S.; Filatreau, J. Occurrence and concentrations of benzotriazole
680 UV stabilizers in marine organisms and sediments from the Ariake Sea, Japan. *Environ.*
681 *Sci. Technol.* **2009**, *43*, 6920–6926.
- 682 (67) Kim, J.-W.; Isobe, T.; Ramaswamy, B. R.; Chang, K.-H.; Amano, A.; Miller, T. M.;
683 Siringan, F. P.; Tanabe, S. Contamination and bioaccumulation of benzotriazole ul-
684 traviolet stabilizers in fish from Manila Bay, the Philippines using an ultra-fast liquid
685 chromatography–tandem mass spectrometry. *Chemosphere* **2011**, *85*, 751–758.
- 686 (68) Paredes, E.; Perez, S.; Rodil, R.; Quintana, J.; Beiras, R. Ecotoxicological evalua-
687 tion of four UV filters using marine organisms from different trophic levels *Isochrysis*
688 *galbana*, *Mytilus galloprovincialis*, *Paracentrotus lividus*, and *Siriella armata*. *Chemo-*
689 *sphere* **2014**, *104*, 44–50.
- 690 (69) Janssen, D. B.; Dinkla, I. J.; Poelarends, G. J.; Terpstra, P. Bacterial degradation of
691 xenobiotic compounds: evolution and distribution of novel enzyme activities. *Environ.*
692 *Microbiol.* **2005**, *7*, 1868–1882.
- 693 (70) Rainieri, S.; Barranco, A.; Primec, M.; Langerholc, T. Occurrence and toxicity of musks
694 and UV filters in the marine environment. *Food Chem. Toxicol.* **2017**, *104*, 57–68.

695 **Graphical TOC Entry**